2024 IEEE International Conference on Robotics and Automation (ICRA 2024)
May 13-17, 2024. Yokohama, Japan

Flight Validation of a Global Singularity-Free Aerodynamic Model for Flight Control of Tail Sitters

Krishna Murali[1], Elena P. Moreno[1], and Leandro R. Lustosa[2]

***Abstract*— This work validates through flight tests a previously developed wide-envelope singularity-free aerodynamic framework, called ϕ-theory, for modeling dual-engine tail-sitting flying-wing vehicles for optimization-based control. The ϕ-theory methodology imposes a specific geometry on aerodynamic coefficients that leads to polynomial differential equations of motion amenable to semidefinite programming optimization. Through ϕ-theory, we illustrate a typical predicted longitudinal and lateral flight envelope of a tail-sitting vehicle, which, while commonplace for fixed-wing aircraft in performance textbooks, is a novel figure that generalizes fixed-wing doghouse plots to tail-sitting vehicles. This flight envelope figure suggests a novel, natural and intuitive remote piloting interface that we validate in flight tests. Furthermore, we further validate ϕ-theory through the computation of flight features in simulation and their subsequent observation in flight tests.**

I. Introduction

Different Unmanned Aerial Vehicle (UAV) architectures generate lift forces differently to cope with distinct mission requirements; for instance, fixed-wing platforms yield high speed and long endurance, while rotary-wing aircraft provide hovering capabilities and short take-off and landing. Combining these two features into a single architecture, a Hybrid Aerial Vehicle (HAV), allows a single vehicle to exploit a wider flight envelope and achieve energetically efficient high-speed cruise flight while still retaining hovering flight capabilities.

This work investigates challenges in modeling and actively stabilizing a particular class of HAVs, namely dual-engine tail-sitting flying-wing aircraft, through an ISAE-SUPAERO-made design called **MAV**ION (see Fig. 1). In particular, the hover-to-cruise forward flight transition phase involves significant changes in **MAV**ION's angle of attack, including undergoing post-stall angles. Additionally, the **MAV**ION encounters near-zero freestream velocity during hover flight, which creates singularities in traditional flight mechanics aerodynamic modeling due to ill-defined angles of attack (i.e., one cannot define airflow direction if there is no relative airflow). This calls for a global singularity-free aerodynamic model [1], as opposed to the traditional freestream velocity, angle-of-attack and sideslip-based Buckingham-Pi formulation. Finally, control challenges also stem from significant changes in the vehicle dynamics during different flight modes.

The commonplace strategy for flight mode transition adopted by commercially available controllers (e.g., the open source PX4 Autopilot) and radio-controlled (RC) model aircraft (e.g., the X-VERT tail sitter [2], [3], [4]) is ballistic, in the sense that the actuators setpoints are a superposition of ad-hoc feedforward fixed trajectories in time plus scheduled controllers. The scheduled controllers are often ad-hoc interpolations of a hover and cruise flight controllers, which in their turn are cascaded Proportional Integral Derivative (PID) controllers. From the pilot's perspective, this reflects into a maneuver that automatically performs mode transition through a flip of a switch in the RC transmitter but precludes controlled recovery in the face of unforeseen disturbances or events during the transition. Similarly, the MIST-UAV [5] uses the PX4's transition algorithm with a state-scheduled mixer to adapt to its active wing folding capability.

In the academic literature, additional control strategies exist. For instance, Ref. [6] develops a tail sitter that uses Incremental Nonlinear Dynamic Inversion (INDI), ϕ-theory, and differential flatness to achieve many nonlinear agile and nonconventional maneuvers. The later work validates ϕ-theory through agile flight tests, whereas the original paper [1] restricted model validation to wind tunnel results. In view of imprecise aerodynamics knowledge during flight mode transition, Adaptive Control techniques could regain the performance lost during the design of overly robust controllers. In particular, Ref. [7] uses a simple aerodynamic model for control design and recovers flight performance by means of a 5-hole probe (for measuring airspeed, angle of attack, and sideslip) and Adaptive Control. Similarly, Ref. [8] employs Active Disturbance Rejection Control for the same purpose. Other approaches [9] forgo the need for an accurate mathematical model altogether using Model-Free Control (MFC) strategies.

On the other hand, previous work [10] analyzes wind disturbance rejection of quad-engine tail-sitting flying-wing aircraft controllers during flight mode transition. While successful for quad-engine platforms, the robustness of such a controller in a dual-engine scenario (as in the **MAV**ION) is to be determined. This hypothesis is further blurred by the fact that dual-engine platforms produce pitch moment through elevon surfaces only, while the quad-engine equivalent benefits from quad-engine-based pitching moment generation. This issue is further complicated in flight mode transition where **MAV**ION trimmed elevon settings are close to saturation [11], and reduced pitch (and roll) control

This work was supported by the ISAE-SUPAERO Foundation.

[1]Graduate Student, Department of Aerospace Vehicles Design and Control, ISAE-SUPAERO, Toulouse, France. {krishna.murali, elena.ponce-moreno}@student.isae-supaero.fr

[2]Associate Professor, Department of Aerospace Vehicles Design and Control, ISAE-SUPAERO, Toulouse, France. leandro.lustosa@isae-supaero.fr

Fig. 1. The **MAV**ION version employed throughout this work at outdoor flight (left), rest (center) and indoor flight in tail-sitting mode (right).

authority is available for the controller. Finally, the later controller remains globally applicable only in cases where the angular velocity controller does not saturate. All the previous caveats suggest a Model Predictive Control (MPC)-based controller for handling saturation issues. MPC design employing the model in Ref. [10], however, could potentially yield inaccurately computed trajectories since the MIST-UAV's aerodynamics model was tuned through the XFLR5 Computer Fluid Dynamics (CFD) software, which linear vortex panel assumptions might yield opposite-sign behavior at post-stall angles of attack. Other quad-engine platforms, such as Vogi [12], have employed CFD simulations with heuristic corrections for modeling. Trajectory generation through optimization of PID controller attitude setpoints through sequential convex optimization is demonstrated in simulation in Ref. [13]; however, its computation time is too long for real-time applications.

These issues motivate using an optimization-friendly dynamics model, namely, the ϕ-theory aerodynamics formulation. ϕ-theory is optimization-friendly since it naturally imposes a global polynomial form to the final equations of motion that invites Sums-of-Squares (SOS) optimization techniques to take place. ϕ-theory also supports tail sitter control design at the Massachusetts Institute of Technology [6], at the École Nationale de l'Aviation Civile [14], and at the Delft University of Technology [15].

Through ϕ-theory, we illustrate the **MAV**ION's predicted longitudinal and lateral flight envelope, which, while commonplace for fixed-wing aircraft in performance textbooks, is a novel figure that generalizes fixed-wing doghouse plots to tail-sitting vehicles. This flight envelope figure suggests a novel, natural, and intuitive remote piloting interface that we validate in flight tests. Furthermore, we further validate ϕ-theory through the computation of flight features in simulation and their subsequent observation in flight tests.

The remainder of the paper is organized as follows: Sec. II describes the **MAV**ION mathematical model and computes its flight envelope and operating points. Sec. III explains the controller architecture, its inputs, and simulation results. Finally, Secs. IV and V show respectively the results of flight tests and summarize our findings.

II. Mathematical Model

Traditionally, in Flight Mechanics, the expression of forces and moments on an airfoil are computed using dimensional analysis. Application of the Buckingham-π theorem to a steady airflow condition yields

$$\begin{aligned} \boldsymbol{F}_{\mathrm{b}} &= \frac{1}{2}\rho S v_{\infty}^2 \boldsymbol{C}_{\mathrm{b}}(\alpha,\beta,M,Re), \\ \boldsymbol{M}_{\mathrm{b}} &= \frac{1}{2}\rho S v_{\infty}^2 B \boldsymbol{K}_{\mathrm{b}}(\alpha,\beta,M,Re) \end{aligned} \tag{1}$$

where $\boldsymbol{F}_{\mathrm{b}}, \boldsymbol{M}_{\mathrm{b}} \in \mathbb{R}^3$ denote, respectively, aerodynamic forces and moments described in the airfoil body frame, and $B = \left[\begin{smallmatrix} b & 0 & 0 \\ 0 & c & 0 \\ 0 & 0 & b \end{smallmatrix}\right]$ where b, c, ρ, $S \in \mathbb{R}_{+}^{*}$ represent the reference wingspan, reference chord, freestream air density, and reference finite wing surface, respectively. $\mathbf{C}_b$ and $\mathbf{K}_b$, both functions mapping $\mathbb{R}^4$ into $\mathbb{R}^3$, represent the aerodynamic coefficients for forces and moments, described in the body frame B. These coefficients depend on dimensionless quantities α, β, M, and Re, corresponding to the angle of attack, sideslip angle, Mach number, and Reynolds number, respectively. In this context, we assume that the airflow with freestream velocity $\mathbf{v}_\infty$ is incompressible and inviscid, rendering $\mathbf{C}_b$ and $\mathbf{K}_b$ function of only α and β across all relevant flight conditions, and computed from $\boldsymbol{v}_\infty = (v_{\infty,\mathrm{b1}}, v_{\infty,\mathrm{b2}}, v_{\infty,\mathrm{b3}})$ according to

$$\begin{aligned} \alpha &= \tan^{-1}\left(\frac{v_{\infty,\mathrm{b3}}}{v_{\infty,\mathrm{b1}}}\right), \\ \beta &= \sin^{-1}\left(\frac{v_{\infty,\mathrm{b2}}}{v_{\infty}}\right) \end{aligned} \tag{2}$$

where $v_\infty = |\boldsymbol{v}_\infty|$ and b1, b2 and b3 are as in Fig. 2. Tail sitter hovering flight scenarios involve near-zero $\boldsymbol{v}_\infty$, especially in wing sections unaffected by the propellers' slipstream. These low velocities result in nearly zero algebraic divisions in Eq. 2, precluding numerical stability and differentiability. In addition, this formulation generally yields non-polynomial differential equations of motion that preclude SOS optimization usage and, thus, time-efficient MPC solvers that explore an optimization problem's algebraic structure.

A. ϕ-theory aerodynamics for tail sitters

The ϕ-theory formulation [1] proposes aerodynamic forces and moments modelization as

$$\boldsymbol{\tau} = \frac{1}{2}\rho S \eta C \Phi(\boldsymbol{\eta}) C \boldsymbol{\eta} \tag{3}$$

where $\boldsymbol{\tau}$, $\boldsymbol{\eta} \in \mathbb{R}^6$ are, respectively, the aerodynamic wrench (with respect to the center of mass) and aerodynamic twist, and, accordingly,

$$\begin{aligned} \boldsymbol{\tau}_{\mathrm{b}} &= \begin{pmatrix} \boldsymbol{F}_{\mathrm{b}} \\ \boldsymbol{M}_{\mathrm{b}} \end{pmatrix}, \\ \boldsymbol{\eta}_{\mathrm{b}} &= \begin{pmatrix} \boldsymbol{v}_{\infty,\mathrm{b}} \\ \boldsymbol{\omega}_{\infty,\mathrm{b}} \end{pmatrix} \end{aligned} \tag{4}$$

where $\eta = |\boldsymbol{\eta}|$ is the aerodynamic ϕ-norm, given by

$$\eta = \sqrt{v_\infty^2 + \phi c^2 \omega_\infty^2}, \quad \phi > 0 \tag{5}$$

where $\phi \in \mathbb{R}$ is a dimensionless tunable parameter. Moreover $\omega_{\infty,\mathrm{b}} = |\boldsymbol{\omega}_{\infty,\mathrm{b}}|$ denotes half of the free-stream vorticity $\boldsymbol{\varepsilon}_\infty$ such that

$$\boldsymbol{\omega}_\infty = \frac{1}{2}\boldsymbol{\varepsilon}_\infty = \frac{1}{2}\boldsymbol{\nabla} \times \boldsymbol{v}_\infty. \tag{6}$$

In the absence of wind, it can be readily demonstrated that $\boldsymbol{\omega}_\infty$ equals the vehicle's angular velocity. Furthermore, the matrix $\mathrm{C} \in \mathbb{R}^{6\times6}$ is an augmented airfoil dimensions reference matrix, and its definition is

$$C = \begin{bmatrix} I_{3x3} & 0_{3x3} \\ 0_{3x3} & B \end{bmatrix}. \tag{7}$$

Finally, $\Phi : \mathbb{R}^6 \to \mathbb{R}^{6\times6}$ is the aerodynamic ϕ-coefficient. Previous work [1] shows that a constant $\Phi(\boldsymbol{\eta}) = \Phi$ is enough to capture dominant features (e.g., post-stall effects, aerodynamics derivatives and global dissipation of energy, over the entire flight envelope).

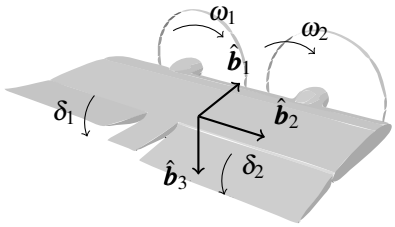

Fig. 2. Perspective view, body-axis definition and actuation inputs for a typical tilt-body vehicle representation.

We encourage the reader to check Ref. [1], where supplementary information (including wing-propeller interaction modeling) is present and further demonstrates the framework viability for dual-engine tail-sitting flying-wing vehicle modeling for control purposes. Herein, we recall that ϕ-theory purposely does not strive for a more precise representation of reality and that other more accurate formulations are present. ϕ-theory focuses on developing a minimal description sufficient for guidance and control using SOS optimization while maintaining reasonable robustness margins requirements on control design.

For the present paper, it suffices to say that the differential equations of motion are in the form $\dot{\boldsymbol{x}} = f(\boldsymbol{x}, \boldsymbol{u})$, where $f(\cdot,\cdot)$ is polynomial, and the state $\boldsymbol{x}(t)$ and input $\boldsymbol{u}(t)$ definitions are

$$\boldsymbol{x} = \begin{pmatrix} \boldsymbol{v}_{\mathrm{b}} & \boldsymbol{\omega}_{\mathrm{b}} & q \end{pmatrix} \tag{8}$$

and

$$\boldsymbol{u} = \begin{pmatrix} \omega_1 & \omega_2 & \delta_1 & \delta_2 \end{pmatrix} \tag{9}$$

where $\boldsymbol{v}_{\mathrm{b}}, \boldsymbol{\omega}_{\mathrm{b}} \in \mathbb{R}^3$, $q \in \mathbb{R}^4$ and $\omega_i, \delta_i \in \mathbb{R}$ are, respectively, drone velocity with respect to the ground described in body frame, drone inertial angular velocity described in body frame, orientation of drone with respect to ground in quaternion formulation, propeller angular velocity and elevon deflection (see Fig. 2). A Quaternion-based parametrization of orientation was chosen since its time derivative equation is polynomial in q and $\boldsymbol{\omega}_{\mathrm{b}}$. Finally, we reinforce that ϕ-theory is not a polynomial Taylor approximation (and thus not local) but a physics-based global polynomial model for the entire flight envelope.

B. Trim points and pilot interface definition

Previous work [1] proposes an efficient trim point solver (namely, ϕ-trim) for the **MAVION** longitudinal envelope. This algorithm proves that, under ϕ-theory modeling assumptions, every achievable airspeed has a unique corresponding state $\boldsymbol{x}$ and input $\boldsymbol{u}$ pair that satisfies the trimming condition $\dot{\boldsymbol{x}} = \boldsymbol{0}$. Furthermore, the algorithm provides the answer for whether or not a particular dual-engine tail-sitting flying-wing drone can fly in a given airspeed. Therefore, the algorithm proves the uniqueness and existence of longitudinal trim points and provides non-iterative steps to compute them without resorting to initial guesses. This tool is also helpful for online planning algorithms [16] that demand real-time and sure computation of trim points.

Banking turn trim points computation is considerably more complicated than its longitudinal counterpart. For instance, ϕ-trim is not extendable to computing trim points during turns and our group is still researching for fast and reliable trimming algorithms. Nevertheless, we propose to use traditional nonlinear numerical solvers with initial guesses initialized by ϕ-trim. We start by formalizing our problem. In the following definition, the subscript l indicates that the vectors are described in the local ground frame.

Definition 1 (Banking turn limit cycles)**.** *A periodic solution $\boldsymbol{x}(t) : \mathbb{R} \to \mathbb{R}^{10}$ actuated by a constant $\boldsymbol{u}(t)$ is called a banking turn limit cycle if*

1) $\dot{\boldsymbol{v}}_l = \boldsymbol{\omega}_l \times \boldsymbol{v}_l$ *(zero tangential acceleration)*
2) $\dot{\boldsymbol{\omega}}_l = \boldsymbol{0}$ *(constant turn rate and curvature)*
3) $v_{l3} = 0$ *(level flight condition)*

We shall conjecture (based on numerical data to be shown shortly) that each banking turn limit cycle is produced by at most one distinct $\boldsymbol{u}$. Therefore, each limit cycle can be identified by its associated (v, ω). Furthermore, the attitude description is periodic in yaw $\psi(t)$, but constant in pitch $\theta(t)$ and roll $\phi(t)$, where roll, pitch and yaw angles are rotations about the body axes in the 3-2-1 Euler angle sequence. Thus we extend the limit cycle description to read $(v, \omega, \boldsymbol{u}, \theta, \phi)$. The set of all limit cycle descriptions for a given ω is denoted by Θ_ω. Furthermore, $\Theta_\omega(v)$ denotes the tuple $(\boldsymbol{u}, \theta, \phi)$ necessary for achieving the (v, ω) banking limit cycle. The set $\{\Theta_\omega(v)\}$ is numerically computed for the

MAVION implementing the `fsolve` routine in MATLAB, and illustrated in Fig. 3, Fig. 4 and Fig. 5.

The points (v, ω) exterior to the illustrated flight envelope failed to converge to a solution in view of our acceptable tolerance or maximum number of `fsolve` iterations. Additionally, notice that we allowed for $-\infty < \omega_i < \infty$ and $-\infty < \delta_i < \infty$. Therefore, the flight envelope is not due to actuators saturation. Instead, we observe that actuator values are well within reasonable values. Therefore, the flight envelope limitation is of banking aerodynamics nature; longitudinal maneuvers such as hover-to-cruise transition fall within this envelope. This argument is upheld by the asymptotic behavior of θ and ϕ level curves in Fig. 5. Finally, it is worth mentioning that ϕ-trim curves support back-of-the-envelope drone design techniques (e.g., choice of payload, wingspan, number of propellers) in view of a desired mission flight envelope. Unlike the trimmed flight doghouse curves of conventional aircraft, the tail-sitting ϕ-trim curves indicate maneuverability and sustained trimmed flight even at and around zero velocity, further illustrating the advantages of its architecture.

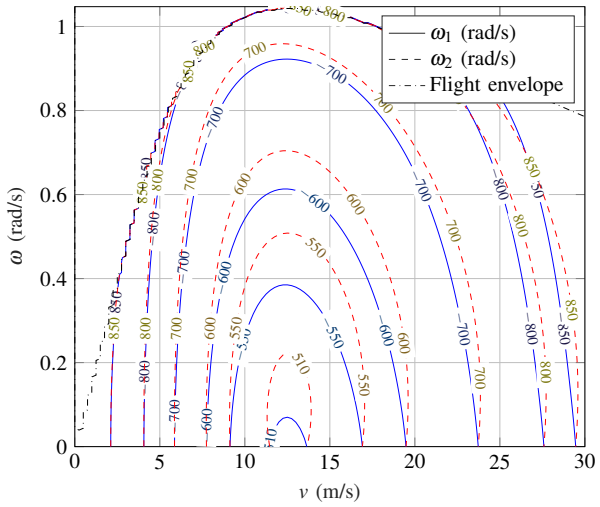

Fig. 3. Lateral-directional equilibrium polars.

Notice that control setpoints (trim points or limit cycles) are unambiguously defined by desired velocities (v, ω). This suggests an intuitive pilot interface for setpoint radio control (RC) where the pilot controls the tail sitter thinking on where it needs to go instead of which orientation it needs to be. This abstracts the internal workings of the drone, relieves piloting efforts and provides ground for straightforward automatic guidance laws. Fig. 6 illustrates our proposition of RC controller input assignment for commonplace RC radio standards.

An equivalent piloting approach to tilt-wing vehicles is heuristically defined in Ref. [17]. We support this line of thought by providing the aforementioned results.

III. Control Architecture

For control, this work expands to lateral flight a previously proposed (and validated in simulation) longitudinal-

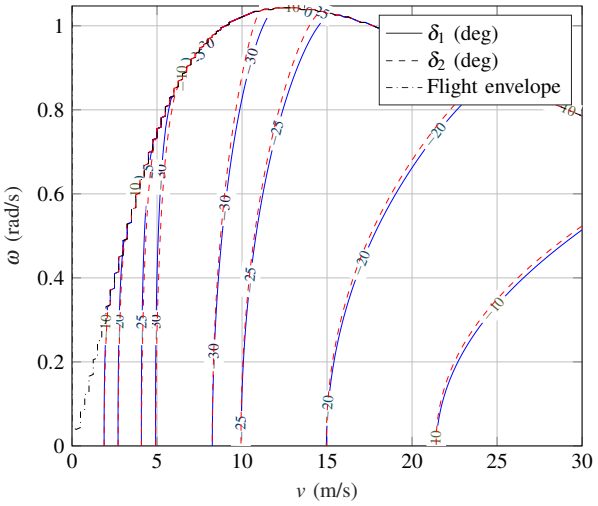

Fig. 4. Lateral-directional equilibrium polars.

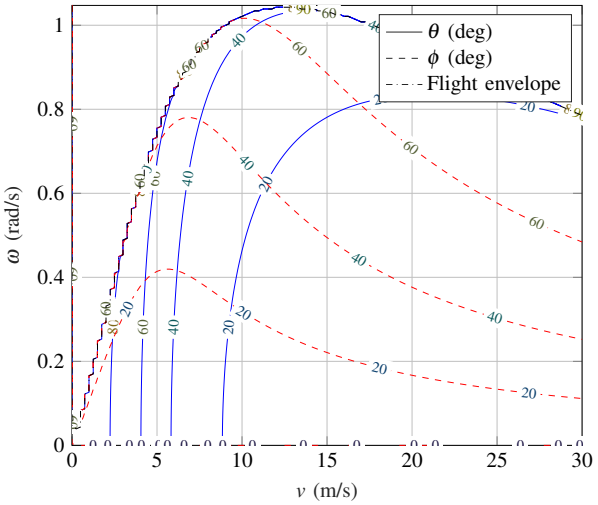

Fig. 5. Lateral-directional equilibrium polars.

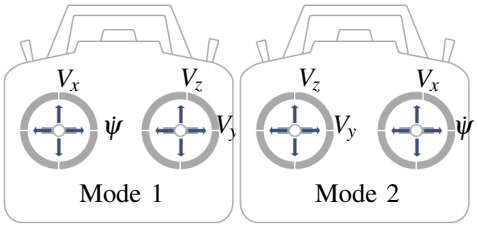

Fig. 6. Input assignments of standard RC radio modes. Notice that $\dot{\psi}$, V_x, V_z and V_y denote, respectively, desired yaw rate with respect to geographic North (which in turn controls the heading), forward velocity, vertical velocity and lateral velocity.

only scheduled Linear Quadratic Regulator (LQR) controller, in which the number and location in the flight envelope of scheduled points are decided via a Region of Attraction analysis [11]. Since quaternions reside in a unitary radius sphere, their linearization always yields uncontrollable systems (the controllable subspace is tangent to the desired quaternion

setpoint). This issue can be solved, for instance, either by local Euler Angle charts or virtual inputs [18]. In this work, we employ local Euler Angle charts.

For each operating point, we design an LQR controller $\Delta\boldsymbol{u} = -K\Delta\boldsymbol{x}$ given an appropriate choice of Q and R (i.e., quadratic cost weights). These are tuned by trial-and-error runs in a computer simulator to account for actuator bandwidth, state estimation imperfections and embedded computer sampling times (all comprised in simulation). Once appropriate Q and R are found for hovering (i.e., $v = \omega = 0$), they are replicated for all other trim points' LQR computations.

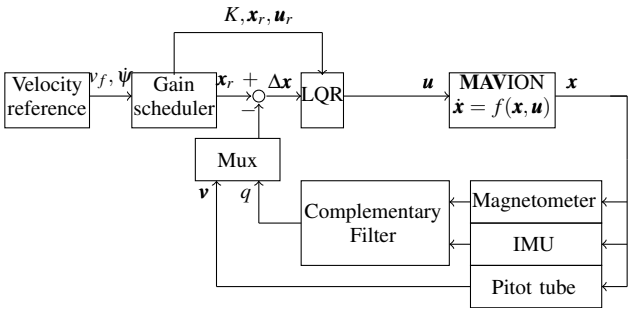

Fig. 7. Block diagram of the `MATLAB/Simulink` simulation setup for the experiment.

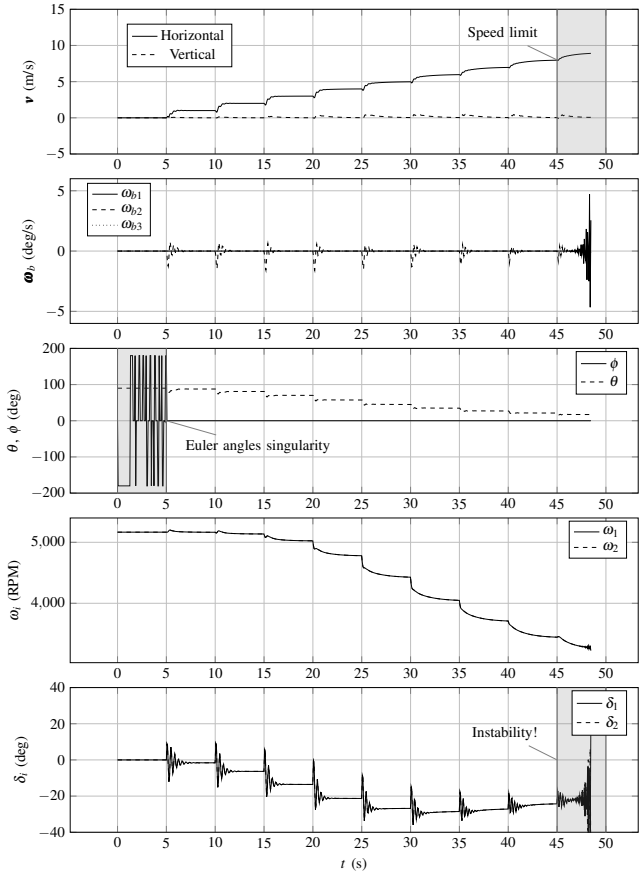

Fig. 8. Flight simulation results with a single LQR controller.

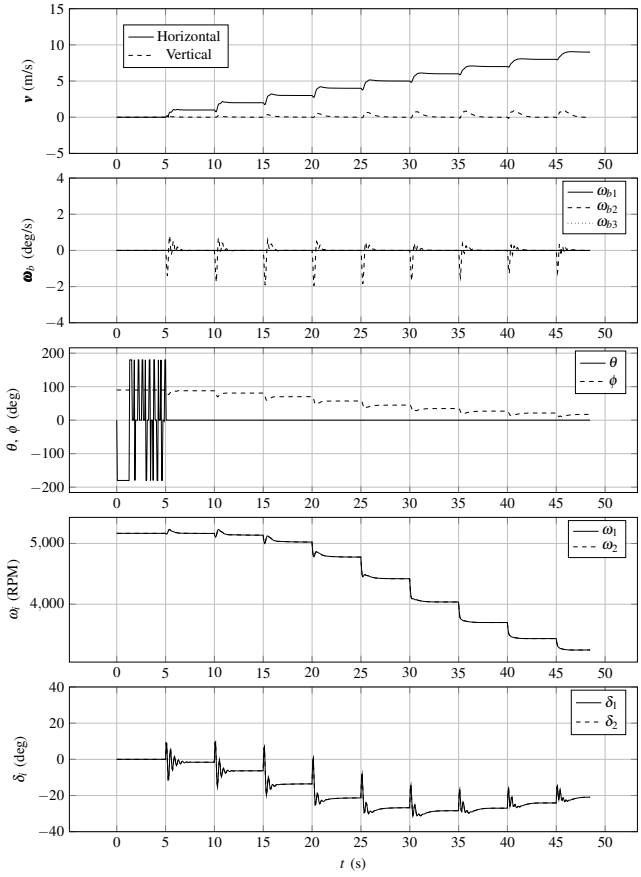

Fig. 9. Flight simulation results with a scheduled LQR controller.

IV. Experimental Results

Beforehand, the typical behavior of a single LQR (tuned for hovering flight) controller during a flight transition maneuver is shown through simulations and real flights. Its shortcomings will be shown to render transition flight impractical and the previously designed gain-scheduled controller is applied instead to stabilize the maneuver. The chosen estimation and control strategy is summarized in Fig. 7.

A. Flight simulation results

The velocity $\boldsymbol{v}$ flight profile pursued by simulation is illustrated in Fig. 8. Notice that velocity is slowly increased by increments of 1m/s to prove stability in several points in the middle of the transition.

Before simulating the full scheduled controller system, it is worth questioning whether gain-scheduling is really necessary. This question is supported by the fact that fixed-wing vehicles are inherently stable[1] and therefore maybe a hover-stabilizing controller would also be suitable for cruise mode. Fig. 8 illustrates the results of such a scenario. While hover is stable as expected, transition flight above 10m/s is unstable. Other choices for Q and R gains were examined

[1] Assuming that the fixed-wing vehicle was designed to be passively stable by choosing an adequate center of mass position.

but yielded similar results. Finally, the instability in δ_i is in agreement with our physical intuition of the system since elevons become more aerodynamically efficient in cruise flight due to the increase of relative airflow.

The scheduled controller, on the other hand and as expected, stabilizes the system for any velocity as Fig. 9 shows. Furthermore, propeller response ω_i illustrates that the system time constants are also kept invariant over all velocities, while time constants are degraded in Fig. 8 as velocity increases.

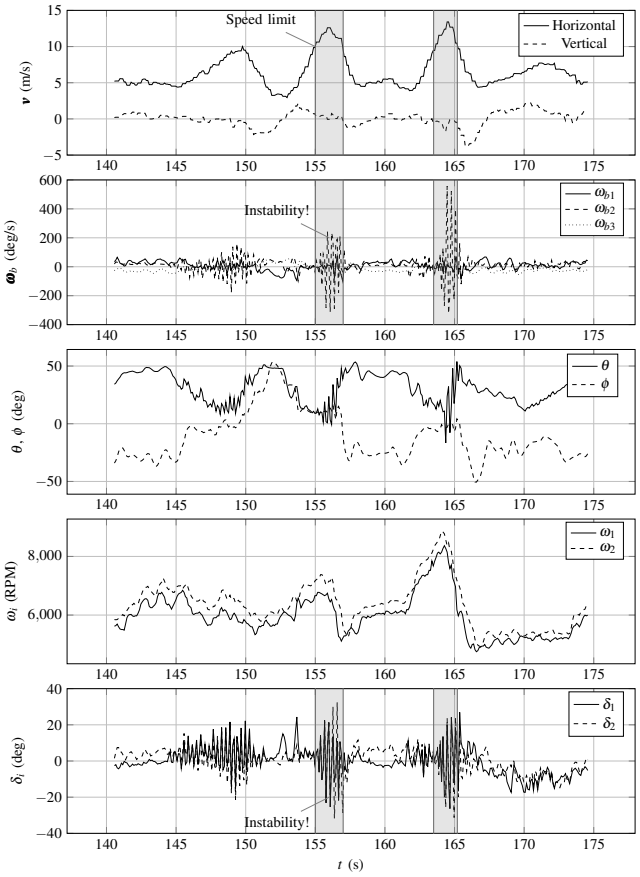

Fig. 10. Flight experiment results with a single LQR controller.

B. Flight test results

Flight tests were conducted to investigate the predicted aforementioned velocity instability limit due to single LQR control design. Fig. 10 illustrates an attempt for transition flight. Indeed, every time vehicle velocity v rises above 10m/s, unstable pitch dynamics appears (see pronounced $\boldsymbol{\omega}_{b2}$, δ_1 and δ_2 undamped oscillations). Therefore, the single LQR controller design is only able to stabilize the vehicle up to 10m/s, and ϕ-theory predictions in simulation matched reality. On its turn, Fig. 11 shows a successful attempt of flight transition through scheduled LQR controllers. Oscillations are no longer present, the cruise velocity was achieved and a back-to-hover maneuver was successfully performed.

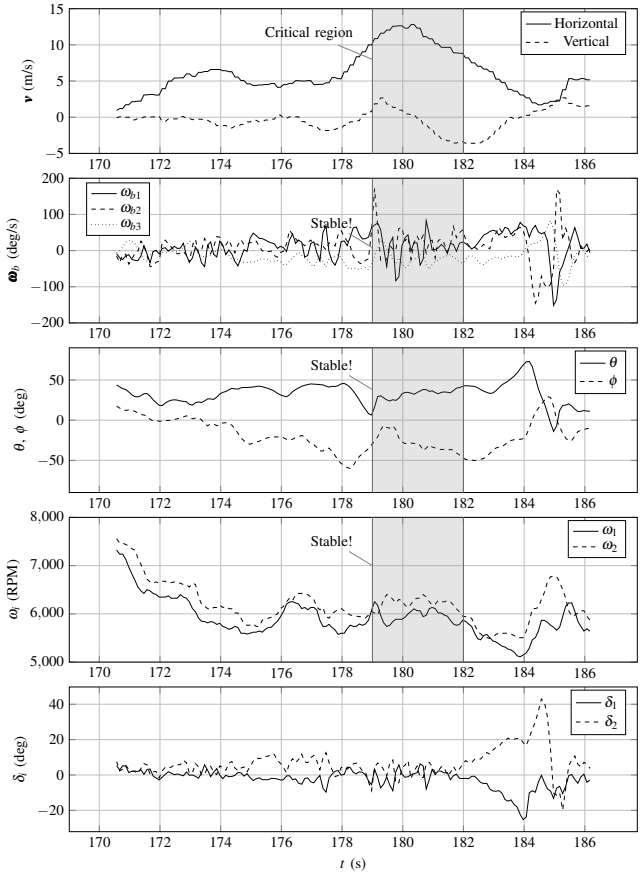

Fig. 11. Flight experiment results with gain-scheduled LQR controllers.

V. Conclusions

A turn performance and agility analysis of the dual-motor tail-sitting flying-wing **MAV**ION vehicle was performed for banked turns, and the associated flight envelope was computed using ϕ-theory. A scheduled LQR controller ensured flight stability during simulation and flight tests for trim points distributed across the flight envelope. Simulation and flight tests confirmed the advantage of employing a model-based gain-scheduled LQR controller. Furthermore, the simulation and flight test findings matched, further validating ϕ-theory. Additionally, our proposed RC transmitter piloting abstraction avoids the necessity of multiple flight modes, homogenizes pilot thinking throughout the flight envelope, and was successfully tested in flight. Future work will involve implementing SOS-based controllers that fully exploit the polynomial nature of ϕ-theory-based models and allow for more agile maneuvers.

References

[1] L. R. Lustosa, F. Defaÿ, and J.-M. Moschetta, "Global singularity-free aerodynamic model for algorithmic flight control of tail sitters," *Journal of Guidance Control and Dynamics*, vol. 42, no. 2, pp. 303–316, 2019, doi: 10.2514/1.G003374.

[2] S. Fuhrer, S. Verling, T. Stastny, and R. Siegwart, "Fault-tolerant flight control of a VTOL tailsitter UAV," *International Conference on Robotics and Automation (ICRA)*, 2019, doi: 10.1109/icra.2019.8793467.

[3] R. Ritz, and R. D'Andrea, "A global strategy for tailsitter hover control," *Springer Proceedings in Advanced Robotics*, 2017, pp. 21–37, doi: 10.1007/978-3-319-51532-8_2.

[4] M. Mousaei, J. Geng, A. Keipour, D. Bai, and S. Scherer, "Design, modeling and control for a tilt-rotor VTOL UAV in the presence of actuator failure," *IEEE/RSJ International Conference on Intelligent Robots and Systems (IROS)*, 2022, doi: 10.1109/iros47612.2022.9981806.

[5] R. D'Sa, and N. Papanikolopoulos, "Design and experiments for MultI-Section-Transformable (MIST)-UAV," *International Conference on Robotics and Automation (ICRA)*, 2019, doi: 10.1109/icra.2019.8793575.

[6] E. Tal, and S. Karaman, "Global incremental flight control for agile maneuvering of a tailsitter flying wing," *Journal of Guidance Control and Dynamics*, vol. 45, no. 12, pp. 2332–2349, 2022, doi: 10.2514/1.G006645.

[7] X. Shi, P. Spieler, E. Tang, E.-S. Lupu, P. T. Tokumaru, and S.-J. Chung, "Adaptive nonlinear control of fixed-wing VTOL with airflow vector sensing," *International Conference on Robotics and Automation (ICRA)*, 2020, doi: 10.1109/icra40945.2020.9197344.

[8] Y. Yang, J. Zhu, X. Zhang, and X. Wang, "Active disturbance rejection control of a flying-wing tailsitter in hover flight," *IEEE/RSJ International Conference on Intelligent Robots and Systems (IROS)*, 2018, doi: 10.1109/iros.2018.8594470.

[9] J. M. O. Barth, J.-P. Condomines, J.-M. Moschetta, A. Cabarbaye, C. Join, and M. Fliess, "Full model-free control architecture for hybrid UAVs," *American Control Conference (ACC)*, 2019, doi: 10.23919/acc.2019.8814993.

[10] X. Lyu, H. Gu, Y. Wang, Z. Li, S. Shen, and F. Zhang, "Design and implementation of a quadrotor tail-sitter VTOL UAV," *International Conference on Robotics and Automation (ICRA)*, 2017, doi: 10.1109/icra.2017.7989452.

[11] L. R. Lustosa, F. Defaÿ, and J.-M. Moschetta, "Longitudinal study of a tilt-body vehicle: Modeling, control and stability analysis," *2015 International Conference on Unmanned Aircraft Systems (ICUAS)*, 2015, doi: 10.1109/icuas.2015.7152366.

[12] R. Chiappinelli, M. Cohen, M. Doff-Sotta, M. Nahon, J. R. Forbes, and J. Apkarian, "Modeling and control of a passively-coupled tilt-rotor vertical takeoff and landing aircraft," *International Conference on Robotics and Automation (ICRA)*, 2019, doi: 10.1109/icra.2019.8793606.

[13] J. Zhou, X. Lyu, Z. Li, S. Shen, and Z. Fu, "A unified control method for quadrotor tail-sitter UAVs in all flight modes: Hover, transition, and level flight," *IEEE/RSJ International Conference on Intelligent Robots and Systems (IROS)*, 2017, doi: 10.1109/iros.2017.8206359.

[14] F. Sansou, and L. Zaccarian, "On local-global hysteresis-based hovering stabilization of the DarkO convertible UAV," *European Control Conference (ECC)*, 2022, doi: 10.23919/ecc55457.2022.9838387.

[15] E. J. J. Smeur, M. Bronz, and G. De Croon, "Incremental control and guidance of hybrid aircraft applied to a tailsitter unmanned air vehicle," *Journal of Guidance Control and Dynamics*, vol. 43, no. 2, pp. 274–287, 2020, doi: 10.2514/1.g004520.

[16] R. Cory, and R. Tedrake, "Experiments in fixed-wing UAV perching," AIAA Guidance, Navigation and Control Conference and Exhibit, 2008, doi: 10.2514/6.2008-7256.

[17] P. Hartmann, C. Meyer, and D. Moormann, "Unified velocity control and flight state transition of unmanned tilt-wing aircraft," *Journal of Guidance, Control, and Dynamics*, vol. 40, no. 6, pp. 1348–1359, 2017, doi: 10.2514/1.G002168.

[18] L. R. Lustosa, F. Cardoso-Ribeiro, F. Defaÿ, and J.-M. Moschetta, "A new look at the uncontrollable linearized quaternion dynamics with implications to LQR design in underactuated systems," *European Control Conference (ECC)*, 2018, doi: 10.23919/ECC.2018.8550415.